

# GRID CONNECTED PWM INVERTER FOR WIND ENERGY SYSTEM BY USING VOLTAGE AND CURRENT CONTROL

<sup>#1</sup>SANKAR BABU POTLURI, Research Scholar, Rayalaseema University

<sup>#2</sup>Dr.T.PURNA CHANDRA RAO , Professor And Dean, HITS COE,RR Dist, Hyderabad.

Department of Electrical and Electronics Engineering

**ABSTRACT:** Smart grid is a newly flourishing research area because of its viable applications and expected to address the drawback of existing grid. Micro grids are the part of the Smart grid and they are designed to supply electricity for a small community such as residential areas, universities or industrial sites. Power electronics plays a vital role for connecting the renewable energy sources to Micro grid system. There is a generic current loop for different modes of operation to ease the transition between different modes, including stand-alone inverter mode, grid-tied inverter mode, ac voltage regulation is of importance because of the sensitive loads In dc-micro grid applications, a power distribution system requires a bi-directional inverter to control the power flow between dc bus and ac grid, and to regulate the dc bus to a certain range of voltages, in which dc load may change abruptly. This will result in high dc-bus voltage variations; the bi-directional inverter can shift its current commands according to the specified power factor at ac grid side. The Simulation results are carried out by Matlab/Simulink to verify the performance of the proposed method.

**Keywords:** Islanding Detection, Micro Grid System, Multifunction Converter, PLL, Single-Phase.

## I. INTRODUCTION

The existing electricity grid converts only one-third of fuel into electricity and 8% of its output is wasted across the transmission lines. Smart grid technology basically derived from traditional power grid with some additional features such as reliability, efficiency and sustainability [1]-[2]. The conventional methods of power generation are burning of fossil fuels which affect the environment, causing an increase in greenhouse gas emissions that leads to global warming. Even though these methods of generations have exceptional scale of economy, it transmits power over long distances [3]. As a result, it has turn into the driving force for the growing interest in alternative energy. Distributed generation is one approach to the manufacture and transmission of electric power. Today photovoltaic (PV) power

systems are becoming more and more popular, with the increase of energy demand and the concern of environmental pollution around the world. Four different system configurations are widely developed in grid-connected PV power applications: the centralized inverter system, the string inverter system, the multi-string inverter system and the module-integrated inverter system. Generally three types of inverter systems except the centralized inverter system can be employed as small-scale distributed generation (DG) systems, such as residential power applications. The most important design constraint of the PV DG system is to obtain a high voltage gain. This paper proposes a photovoltaic (PV) system, which presents a set of advantages when compared to conventional stand-alone PV system. In the proposed system, the generated energy by the PV arrays is processed by multistring step-up converters.

## II. SYSTEM MODES OF OPERATION: MODELING AND CONTROL STRUCTURE

Before the control structure is designed and implemented, the converter system needs to be modeled. Specifically, the full bridge, multifunctional PWM converter with different possible ac or dc configurations is shown in Fig.1, where  $i_{dg}$  is the current flowing from the dc DG resources, and its average model of full-bridge is described in (1) and (2).

$$v_{AB} = d_{ab}v_{dc} \quad (1)$$

$$i_{dc} = d_{ab}i_{ac} \quad (2)$$

As seen in (1) and (2),  $v_{AB}$ ,  $i_{dc}$  and  $d_{ab}$  are the average terminal voltage of the full bridge, average dc-link current, and average duty-cycle varying between -1 and 1, respectively. Notice that if  $v_{dc}$  is constant, the terminal voltage  $v_{AB}$  is only a function of the duty-cycle  $d_{ab}$ . The differential equations describing the average model of the full-bridge converter may then be derived as follows:

$$L_{ac} \frac{di_{ac}}{dt} = v_{AB} - v_{ac} \tag{3}$$

$$C_{ac} \frac{dv_{ac}}{dt} = i_{ac} - \frac{v_{ac}}{Z_{ac}} \tag{4}$$

$$C_{dc} \frac{dv_{dc}}{dt} = i_{dg} - \frac{v_{dc}}{Z_{dc}} - i_{dc} \tag{5}$$

$$H_{delay} = e^{-sT_{delay}} = \frac{1 - 0.5sT_{delay} + \frac{(sT_{delay})^2}{12}}{1 + 0.5sT_{delay} + \frac{(sT_{delay})^2}{12}}, T_{delay} = T_{sample} \tag{7}$$

### III. GENERIC INNER AC CURRENT LOOP DESIGN

The average and small-signal models for the different modes can be derived by combining (1)–(5). Notice that in GCM, the dynamics of the ac capacitor can be ignored due to the stiff grid, just as the dynamics of the dc-link capacitor can be ignored because of the constant dc-link voltage during SAM. With the control architecture selected to be a doubleloop feedback system, as shown in Fig.1, the inner loop is used to regulate the ac line inductor current. In order to achieve fast dynamic responses from a wide array of disturbances, the inner loop will need to be designed with high bandwidth, while the outer loops regulate different control variables depending on the operating mode. Inclusion of all control features, such as digital delays and sensor filters should also be included. Each sensor filter is assumed to be a second-order, low-pass-filter, Hfilter(6). A one switching-cycle ( $T_{sample}$ ) delay, Hdelay(7), is modeled in the modulator to approximate the digital computation and A/D conversion delay. The modulator gain is assumed to be unity

It is worthwhile to demonstrate that the same current loop compensator can be designed and shared by all modes. Specifically, for GCM inverter mode the small-signal transfer function from control-to-current can be simply obtained from the average model given by (1)–(3) and applying a smallsignal perturbation, of which the result is as follows

$$G_{id1}(s) = \frac{\hat{i}_{ac}}{\hat{d}_{ab}} = V_{dc} \frac{1}{sL_{ac}} \tag{8}$$

Notice that (8) is obtained by assuming the small-signal grid voltage is zero due to the stiff grid condition. For the SAM, the transfer function from control-to-current is obtained from the average model described by (1)–(4):

$$G_{id2}(s) = \frac{\hat{i}_{ac}}{\hat{d}_{ab}} = V_{dc} \frac{1 + sZ_{ac}C_{ac}}{Z_{ac} + sL_{ac} + s^2L_{ac}Z_{ac}C_{ac}} \tag{9}$$

$$H_{filter} = \frac{1}{\left(\frac{s}{2\pi f_o}\right)^2 + \left(\frac{s}{Q2\pi f_o}\right) + 1} \tag{6}$$

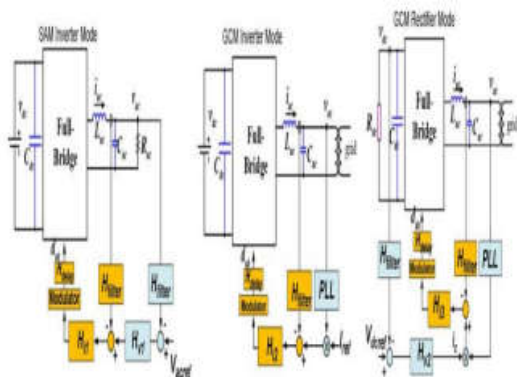


Fig.1. Control structures under different modes of operation

Although SAM does not have a constant operating point for the —outputl, the small-signal model is linear timeinvariant when dc-link voltage is constant. For the GCM rectifier mode however, since there is no fixed operating point and no constant dc-link voltage, the dynamics of both sides of the bridge have to be considered. The result is that there is not a complete accurate small-signal model that can describe the entire dynamics from dc up through the Nyquist frequency [15]. However, if the current loop is modeled in a higher frequency range and the voltage loop in a lower frequency range separately, following the quasi-static modeling approach proposed in [15], the high-frequency small-signal current loop can be modeled since the all the operating points (60 Hz) and varying dc-link voltage (120 Hz) can be assumed to be in steady state because of the high current loop control bandwidth. Hence, can be perturbed as usual for all operating points, and the control-to-current transfer function is then derived as below. The detailed derivation can be found.

$$G_{i_{d3}}(s) = \frac{\dot{i}_{ac}}{\dot{d}_{ab}} = V_{dc} \frac{2 + sZ_{dc}C_{dc}}{d_{ab}^2 Z_{dc} + sL_{ac} + s^2 Z_{dc}L_{ac}C_{dc}} \quad (10)$$

With the transfer functions described in (8)–(10), the current compensator can be designed; but the varying nature of the resultant transfer functions must be considered given that it changes under varying line and load conditions, actual operating mode, and even the converter operating point itself. A comprehensive linear design can still be carried out however, if the control-to-current transfer function is closely examined under these different conditions.

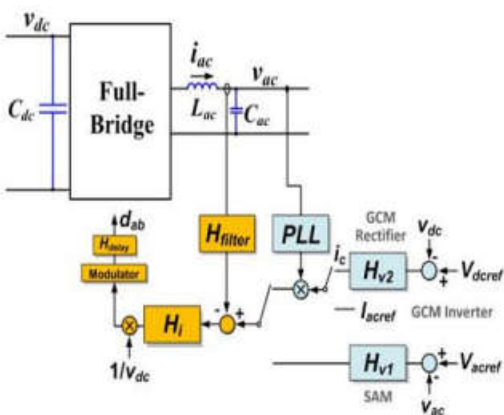


Fig.2. Multi-functional converter control system.

The current loop compensator is designed under SAM light load conditions based on (9). The current PID compensator has the following structure in (11) to compensate the current loop gain in (12).

$$H_i(s) = K \frac{(s + z_1)(s + z_2)}{s(s + p_1)(s + p_2)} \quad (11)$$

$$H_{i-o}(s) = H_{filter}(s) \cdot H_{delay}(s) \cdot G_{i2}(s) \cdot H_i(s) \quad (12)$$

The zeros in(11) are placed around the resonant frequency to compensate the drop in phase, and two poles are used to attenuate the high frequency resonance from grid impedance. The gain, K, is used to achieve the desired loop-gain and bandwidth for the inner current loop. The designed current loop bandwidth is around 2 kHz. As seen, by using a generic current controller one control system can be used for different modes of operation, as shown in Fig.4. Per (8)–(10), a feed-forward loop is also applied to measure the dc-link voltage (Fig.2) and decouple the dc gain from vdc.

#### IV. OUTER LOOP CONTROLLER DESIGN

##### A. Stand-Alone Inverter Mode

The outer loop in this case is an ac voltage loop; as such, the ac-current to ac-voltage transfer function is given by (13) assuming a resistive load.

$$G_{vi\_SAM}(s) = \frac{\dot{v}_{ac}}{\dot{i}_{ac}} = \frac{R_{ac}}{1 + sR_{ac}C_{ac}} \quad (13)$$

The open-loop gain to design the outer voltage compensator is shown in(14),where Gi-c and Gviare the closed-loop current transfer-function, and ac-current to acvoltage transfer function, respectively

$$H_{v-o} = H_{i-c}(s) \cdot G_{vi}(s) \cdot H_{filter}(s) = \frac{G_{i-o}(s)}{G_{i-o}(s) + 1} \cdot G_{vi}(s) \cdot H_{filter}(s) \quad (14)$$

##### B. Rectifier Mode

Dc-link voltage loop controller is designed under the assumption of the previously designed high-bandwidth current loop. Since the dc-link voltage loop bandwidth must be much lower than the frequency of the dc-link voltage ripple (120 Hz). Thus, taking the rms value of vac as the steady-state operating point, the power balance between the ac and dc side of the converter is used to model the voltage loop, which can be found for detailed derivation. If a resistive load is connected, the outer loop transfer function becomes (15), where is the scaling factor of the PLL.

$$G_{vi\_GCM}(s) = \frac{\dot{v}_{dc}}{\dot{i}_c} = \frac{V_{acRMS}^2}{hV_{dc}} \frac{R_{dc}}{2 + sR_{dc}C_{dc}} \quad (15)$$

The outer loop compensators of stand-alone mode and rectifier mode are shown in (16) and (17), respectively

$$H_{v1}(s) = K \frac{(s + z_1)(s + z_2)}{s(s + p_1)(s + p_2)} \quad (16)$$

$$H_{v2}(s) = K \frac{(s + z_1)}{s(s + p_1)} \quad (17)$$

The design criteria of (16) is similar as the current loop design, In (17), zeros is placed specifically to cancel the pole in (15), while another pole is placed after the crossover frequency to attenuate the loop gain at 120 Hz.

**V. MATLAB/SIMULINK RESULTS**

Simulation results of this paper is shown in Figs.3 to 12.

**Case I: Standalone Mode**

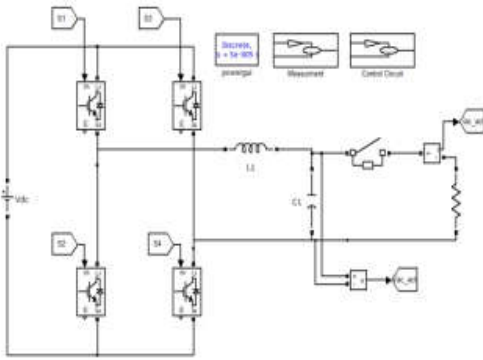


Fig.3. Simulink circuit for standalone mode.

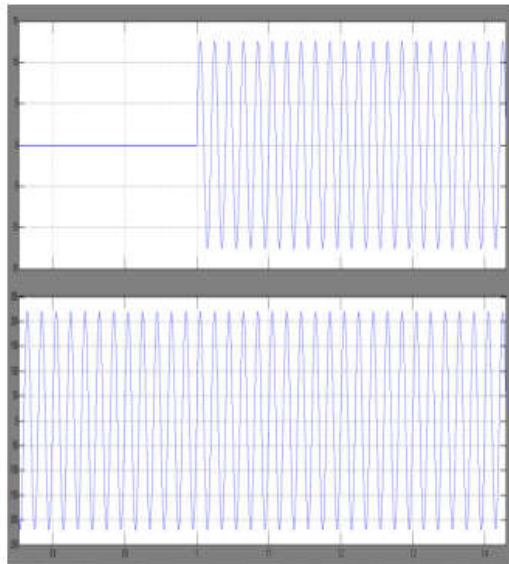


Fig.4. Simulation results for current and voltage waveforms.

**Case II: Grid Connected Mode Inverter**

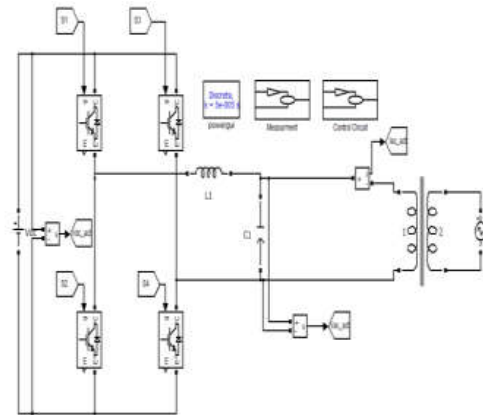


Fig.5. Simulink circuit for grid connected inverter.

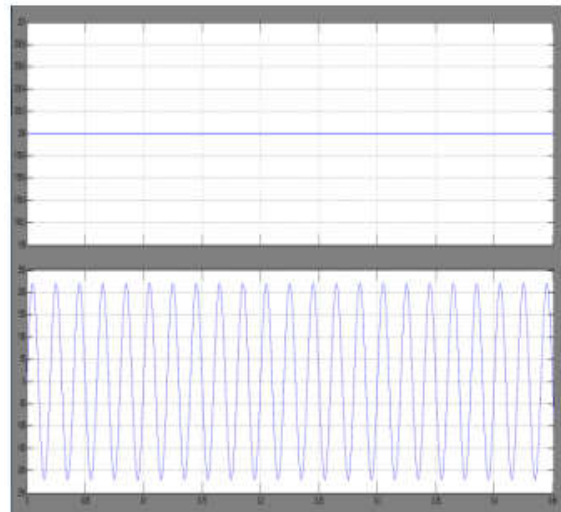


Fig.6. simulation results for dc link voltage and inverter voltage.

**Case III: Grid Connected Rectifier**

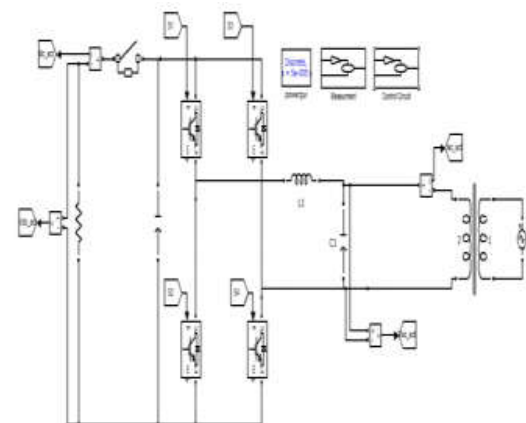


Fig.7. Simulink circuit for grid connected rectifier.

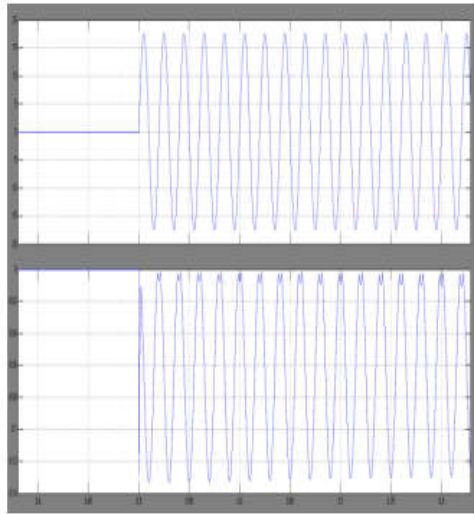


Fig.8.  $i_{ac}$  and  $V_{dc}$  wave forms

**Case IV: Voltage and Current Control of Grid And Island Mode**

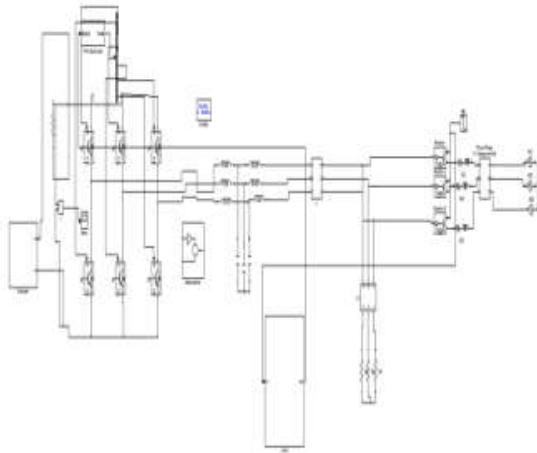


Fig.9. Simulink circuit for voltage and current control of grid and island mode

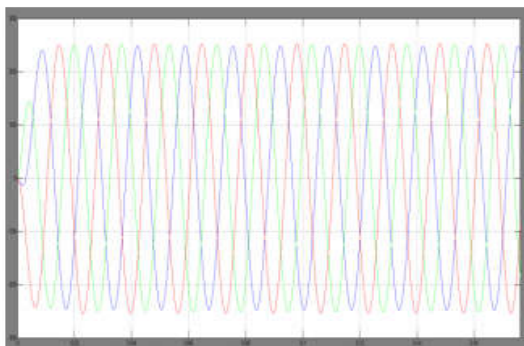


Fig.10. Output waveform of Three phase input voltage.

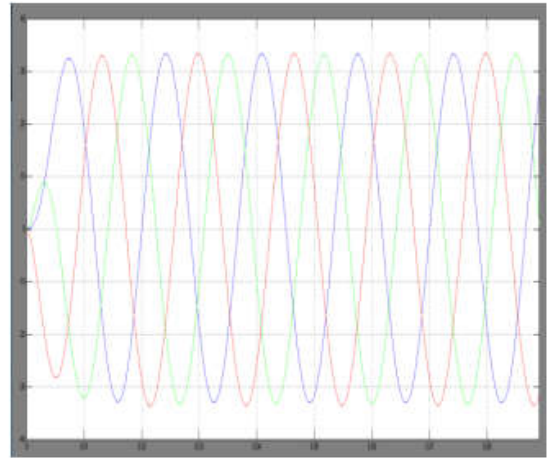


Fig.11. Output waveform of Three phase currents.

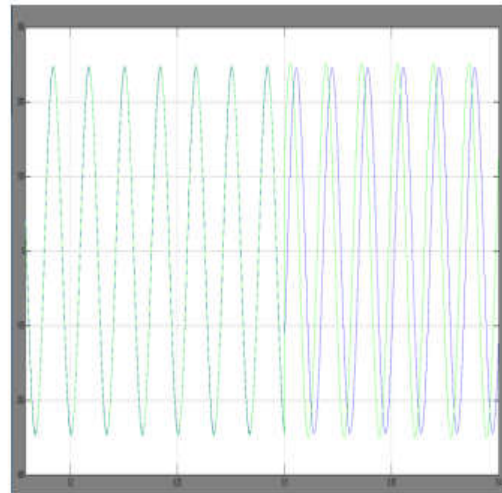


Fig.12. output waveform of the three phase input voltage and grid voltage.

**VI. CONCLUSION**

This paper proposed a complete modeling and control system for a bidirectional, single-phase, multifunctional PWM converter for residential power level distributed renewable energy and grid connected micro grid system applications. A simple control structure was used to cover all of the required operating modes, including stand-alone (SAM), grid-connected (GCM) inverter, and rectifier mode. A new single-phase PLL and active islanding detection algorithm was also proposed for system-level operation in order to meet IEEE standard 1547.

The resulting control structure is very simple and presents robust, low transient responses even for extreme load steps between no-load and heavy-load conditions

## REFERENCES

[1] Y. Li, D. M. Wilathgamuwa, and P. C. Loh, —A grid interfacing power quality compensator for three-phase three wire microgrid applications,|| IEEE Trans. Power Electron., vol. 21, pp. 1021–1031, Jul. 2006.

[2] F. Katiraei and M. R. Iravani, —Power management strategies for a microgrid with multiple distributed generation units,|| IEEE Trans. Power Syst., vol. 21, pp. 1821–1831, Nov. 2006.

[3] D. Boroyevich, I. Cvetkovic, D. Dong, R. Burgos, F. Wang, and F. C. Lee, —Future electronic power distribution systems—a contemplative view,|| in Proc. 2010 IEEE Int. Conf. Optim. Electr. Electron. Equip., pp. 1369–1380.

[4] D. Salomonsson and A. Sannino, —Low-voltage DC distribution system for commercial power systems with sensitive electronic loads,|| IEEE Trans. Power Del., vol. 22, pp. 1620–1627, Jun. 2007.

[5] T. Zhou, P. Li, and B. Francois, —Power management strategies of a DC-coupled hybrid power system in a microgrid for decentralized generation,|| in Proc. 2009 Eur. Conf. Power Electron. Appl., pp. 1–10.

[6] E. Ortjohann, A. Mohd, A. Schmelter, N. Hamsic, and M. Lingemann, —Simulation and implementation of an expandable hybrid power system,|| in Proc. 2007 IEEE Int. Symp. Ind. Electron., pp. 377–382.

[7] I. Cvetkovic et al., —Future home uninterruptible renewable energy system with vehicle-to-Grid technology,|| in Proc. 2009 IEEE Energy Conv. Congr. Expo., pp. 2675–2681

[8] Z. Ye, A. Kolwalkar, Y. Zhang, P. Du, and R. Walling, —Evaluation of anti-islanding schemes based on nondetection zone concept,|| IEEE Trans. Power Electron., vol. 19, pp. 1171–1176, Sep. 2004.

[9] IEEE Standard for Interconnecting Distributed Resources With Electric Power Systems, , IEEE Std 1547-2003

[10] H. M. Kojabadi, B. Yu, I. A. Gadoura, L. Chang, and M. Ghribi, —A novel DSP-based current-controlled PWM strategy for single-phase grid connected inverters,|| IEEE Trans. Power Electron., vol. 21, pp. 985–993, Jul. 2006

[11] H. Gu, Z. Yang, D. Wang, and W. Wu, —Research on control method of double-mode inverter with grid-connection and stand-alone,|| in Proc. 2006 IEEE Power Electron. Motion Control Conf., pp. 1–5

[12] Y.-Y. Tzou, S.-L. Jung, and H.-C. Yeh, —Adaptive repetitive control of PWM inverters for very low THD AC voltage regulation with unknown loads,|| IEEE Trans. Power Electron., vol. 14, pp. 974–981, Sep. 1999.

[13] S.-L. Jung and Y.-Y. Tzou, —Sliding mode control of a closed-loop regulated PWM inverter under large load variations,|| in Proc. 1993 IEEE Power Electron. Specialists Conf., pp. 616–622.

[14] Y. Nishida, O. Miyashita, T. Haneyoshi, H. Tomita, and A. Maeda, —A predictive instantaneous-current PWM controlled rectifier with AC-side harmonics current reduction,|| IEEE Trans. Ind. Electron., vol. 44, pp. 337–343, Jun. 1997

[15] C. Zhou and M. M. Jovanovic, —Design trade-offs in continuous current-mode controlled boost power-factor correction circuits,|| Proc. 1992 Virginia Power Electron. Seminar, pp. 57–68.